KSHV uses viral IL6 to expand infected immunosuppressive macrophages

Michiko Shimoda[1, 2, *], Tomoki Inagaki[1], Ryan Davis[3], Alexander Merleev[1], Clifford G. Tepper[2, 4], Emanual Maverakis[1, 2], and Yoshihiro Izumiya[1, 2, 5, *]

[1] Department of Dermatology, School of Medicine, University of California, Davis, Sacramento, CA USA
[2] UC Davis Comprehensive Cancer Center, Sacramento, CA USA
[3] Department of Pathology and Laboratory Medicine, School of Medicine, University of California, Davis, Sacramento, CA USA
[4] Department of Biochemistry and Molecular Medicine, School of Medicine, UC Davis, Sacramento, California USA
[5] Department of Biochemistry and Molecular Medicine, School of Medicine, University of California, Davis, Sacramento, CA USA

*Correspondence:
Michiko Shimoda PhD
Address: UCDMC Research III Room 3100A, 4645 2nd Avenue, Sacramento CA 95817
E. mail: mshimoda@ucdavis.edu
Current Address: Room 310, Building 100, 1001 Potrero Ave, Division of Experimental Medicine, UCSF, San Francisco, CA 94110, USA
E. mail: michiko.shimoda@ucsf.edu
Phone: 628-206-5232

Yoshihiro Izumiya DVM, PhD
Address: UCDMC Research III Room 2200B, 4645 2nd Avenue, Sacramento CA 95817
E. mail: yizumiya@ucdavis.edu
Phone: 916-734-7253

Running Title

KSHV dysregulates monocytes via vIL6

Summary

KSHV causes multiple inflammatory diseases, however, the mechanism is not clear. Shimoda et al. demonstrate that KSHV preferentially infects monocytes and utilizes virally encoded IL6 to expand and deregulate infected monocytes. This helps the virus escape from host immune surveillance.

Abstract

Kaposi's sarcoma-associated herpesvirus (KSHV) is an oncogenic double-stranded DNA virus and the etiologic agent of Kaposi's sarcoma and hyperinflammatory lymphoproliferative disorders. Understanding the mechanism by which KSHV increases the infected cell population is crucial for curing KSHV-associated diseases. Here we demonstrate that KSHV preferentially infects $CD14^+$ monocytes and sustains viral replication through the viral (v)IL6-mediated activation of STAT1 and 3. Using vIL6-sufficient and vIL6-deficient recombinant KSHV, we demonstrated that vIL6 plays a critical role in promoting the proliferation and differentiation of KSHV-infected monocytes into macrophages. Those macrophages from vIL6-sufficient (wild type) KSHV infection showed a distinct transcriptional profile of elevated IFN-pathway activation with immune suppression and were compromised in T-cell stimulation function compared to those from vIL6-deficient KSHV infection or uninfected control. These results highlight a clever strategy, in which KSHV utilizes vIL6 to secure its initial viral pool by expanding infected dysfunctional macrophages. This mechanism also facilitates KSHV to escape from host immune surveillance to establish a lifelong infection.

61 **Introduction**

62

63 A virus is an infectious agent that can only replicate within a living host organism. Because of
64 this dependence, viruses have evolved various mechanisms to exploit normal cell functions to
65 escape from host immune surveillance for their survival advantage. This exploitation sometimes
66 associates with prolonged damage to the host leading to pathology and diseases caused by the
67 viral infection (Hoenen and Groseth, 2022).

68 Kaposi's sarcoma (KS)-associated herpesvirus (KSHV), or human gamma herpesvirus 8
69 (HHV-8), is an oncogenic double-stranded DNA virus that establishes a lifelong latent infection
70 (Cesarman et al., 2019). KSHV is the etiologic agent of Kaposi's sarcoma and is associated with
71 two lymphoproliferative disorders: multicentric Castleman's disease (MCD) and AIDS-
72 associated primary effusion lymphoma (PEL). KSHV-inflammatory cytokine syndrome (KICS)
73 may also represent a prodromic form of KSHV-MCD, which exhibits elevated KSHV viral loads and
74 circulating inflammatory cytokines including IL-6, IL-10, and a KSHV-encoded IL-6 homolog (vIL-6)
75 (Alomari and Totonchy, 2020; Caro-Vegas et al., 2020; Dumic et al., 2020; Goncalves et al., 2017;
76 Polizzotto et al., 2012; Polizzotto et al., 2016). These highly inflammatory diseases are devastating, and
77 a leading cause of cancer deaths in AIDS patients. Therefore, understanding the mechanism of KSHV
78 infection is crucial for finding a cure for these diseases.

79 Natural transmission of KSHV most likely occurs through salivary and sexual
80 transmission or during transplantation of KSHV-positive organs into a naïve recipient although
81 initial KSHV infection is normally asymptomatic (Cesarman et al., 2019; Dittmer and Damania,
82 2019). In experimental settings, KSHV has been shown to infect various types of cell lines and
83 primary cells such as epithelial cells and immune cells that include B cells, monocytes, and
84 dendritic cells through binding to specific cell surface receptors such as Siglec DC-SIGN
85 (Decker et al., 1996; Gregory et al., 2012; Rappocciolo et al., 2006; Staskus et al., 1997; van der
86 Meulen et al., 2021). However, it remains unclear whether KSHV may preferentially infect a certain
87 cell type among PBMC. The mechanisms by which KSHV facilitates a lifelong infection by
88 increasing viral reservoirs and impacts on the host immune system are also not entirely clear.

89 KSHV-encoded viral interleukin-6 (vIL6) is a homolog of human interleukin-6, which is
90 encoded by KSHV ORF-K2 and is highly expressed during the lytic replication cycle (Sakakibara and
91 Tosato, 2011). Viral IL6 is also expressed at physiologically functional levels in latently infected cells

92 (Chandriani and Ganem, 2010) and is detectable in the sera and/or tumor tissues of patients with KS,
93 PEL, and MCD (Aoki et al., 2001). Viral IL6 enhances cell proliferation, endothelial cell migration,
94 and angiogenesis, leading to tumorigenesis, and has been suggested to be a driver of KICS (Giffin et
95 al., 2015; Zhu et al., 2014). In addition, vIL6 transgenic mice develop IL6-dependent MCD-like disease
96 (Suthaus et al., 2012) and supported tumor metastasis in a murine xenograft model (Fullwood et al.,
97 2018). Mechanistically, vIL6 directly binds to the gp130 subunit of the IL6 receptor without the need
98 of the IL6 receptor, and active the JAK/STAT pathway to induce STAT3 phosphorylation and
99 acetylation (Alomari and Totonchy, 2020; Cojohari et al., 2020; Molden et al., 1997). In addition, vIL6
100 activates the AKT pathway to promote numerous oncogenic phenotypes (Giffin et al., 2015; Morris et
101 al., 2008; Morris et al., 2012; Zhu et al., 2014). STAT3 activation by vIL6 also increases the VEGF
102 expression through the downregulating caveolin 1 (Alomari and Totonchy, 2020) and promotes
103 angiogenesis, suggesting that vIL6 through STAT activation plays an important role in tumorigenesis.
104 Given that the prototype human IL6 plays a critical role in immune regulation and inflammation, vIL6
105 is thought to play a pivotal role in inflammatory KSHV diseases. Here we reveal the role of vIL6 in the
106 regulation of monocytes with recombinant KSHV and de novo infection to the peripheral blood
107 mononuclear cells.
108
109

110 **Results and Discussion**

111

112 **KSHV preferentially infects CD14+ monocytes among PBMC and triggers an inflammatory**
113 **response and macrophage differentiation.**

114

115 To study cell type-specific KSHV infection, we employed a single cell (sc)RNA-seq analysis approach.
116 Recombinant KSHV was purified after two serial ultracentrifugations from the culture supernatant of
117 iSLK.291 cell line, an inducible recombinant KSHV producer. PBMCs were infected with rKSHV.291
118 at MOI=1, fixed at various time points (day 0, 1, 2, and 4) after infection, and subjected to scRNA-seq
119 analysis. KSHV infection and lytic replication in single cells were then monitored by the expression of
120 K2 that encodes vIL6.

121 As shown in Fig. 1A, unsupervised, Uniform Manifold Approximation and Projection (UMAP)
122 for dimension reduction analysis identified 9 clusters among peripheral blood mononuclear cells
123 (PBMCs), each of which can be associated with known immune cell subsets based on corresponding
124 lineage-specific gene expression. Thus, *KLRD1(CD94), CD14, APOBEC3A, VMO1, CD79A*, and *CD3E*
125 genes were used as a marker for NK cells, monocytes, intermediate monocytes, non-classical monocytes,
126 B cells, and T cells, respectively, based on the immune cell data available from the Human protein atlas
127 (Uhlen et al., 2019). As shown in Fig. 1B, *de novo* KSHV infection of PBMCs in conjunction with
128 scRNA-seq analysis at 1-day post-infection (dpi) revealed that K2 (vIL6) expression was almost
129 completely overlapped with CD14 expression. It should be noted that although scarcely K2 expression
130 was also found in $CD79A^+$ B cell, $KLRD1^+$ NK and $CD3E^+$ T cell clusters. KSHV has been shown to
131 establish latent infection in B cells, causing B-cell lymphoma (Cesarman et al., 2019). However, the
132 correlation expression of CD14 and K2 was highly significant (p=8e-191) compared to that of CD19 and
133 K2 (p=0.065) at 1 dpi. The following kinetic scRNA-seq analysis also showed that K2 and CD14 gene
134 expression were colocalized during 1 to 4 dpi (Fig. 1C). In this experiment, the culture medium was not
135 replenished during the period. Infectious KSHV virions that remained in the culture or were newly
136 released from infected cells could have infected other cell subsets of PBMC besides $CD14^+$ monocytes.
137 Thus, KSHV may re-infect $CD14^+$ monocytes and monocytes can support KSHV lytic replication
138 along with vIL6 gene expression. The kinetic scRNA-seq analysis also revealed that KSHV infection
139 in $CD14^+$ monocytes triggered the activation and inflammatory response immediately after KSHV
140 infection at 1dpi as evidenced by the upregulation of *IL3RA* (CD123), *CCL2*, and *TNF*α (Fig. 1C). The

141 latter was followed by the expression of genes associated with differentiation of M2-like macrophages
142 with the suppressive phenotype (*CD274/PD-L1*, *C1QA*, *RNASE1*, *IL-10*, and *CD163*) during 2-4 dpi
143 (Fig. 1D). Collectively, scRNA-seq analysis demonstrates that KSHV preferentially infects $CD14^+$
144 monocytes among PBMCs and triggers monocyte inflammatory response followed by macrophage
145 differentiation program.
146
147
148 **KSHV infection of PBMC triggers STAT activation in dendritic cells and myeloid cell lineages.**
149
150 As a counterpart of pleiotropic cytokine human IL6, viral IL6 has been shown to exhibit multifunctional
151 pathologic roles in KS diseases (Sakakibara and Tosato, 2011). Therefore, we next studied the role of
152 vIL6 in monocyte activation and differentiation using the *de novo* PBMC infection model. To this end,
153 we generated recombinant KSHV lacking vIL6 expression by inserting stop codons in vIL6 with BAC16
154 (vIL6STOP). We also generated a revertant KSHV with intact vIL6 expression (vIL6REV) by changing
155 the sequence back to the original wild-type sequence with BAC recombination. The lack of vIL6
156 expression in vIL6STOP was confirmed by Western blotting using a monoclonal antibody against vIL6
157 (a kind gift from Dr. Robert Yarchoan, NIH) (SFig. 1A).
158 First, to evaluate the signaling events triggered by KSHV infection in immune cells, PBMC from
159 healthy donors (n=6, 3 males and 3 females) were infected with vIL6REV (with vIL6 expression) or
160 vIL6STOP (without vIL6 expression) (MOI=1), or mock-infected (PBS). At 1 dpi, cells were fixed and
161 subjected to CyTOF analysis using a 27-color signaling panel that can differentiate 25 immune cell
162 subsets (SFig. 2). The expression levels of 10 signaling molecules were then determined to evaluate the
163 early signaling events in PBMCs upon KSHV infection.
164 Unsupervised t-distributed stochastic neighbor embedding (tSNE) for dimension reduction
165 analysis was applied for each infection group after 1000 events from 6 samples in each group were
166 concatenated. As shown in Fig. 2A, immune cell subsets were clustered based on each marker
167 expression, and the phenotypic changes induced by infection were visualized and identified by
168 comparison between vIL6STOP, vIL6REV, and mock-infected (PBS) control group (Fig.2 B). The
169 landscape of immune cell phenotype visualized by the tSNE cell clustering was remarkably similar
170 between vIL6STOP and vIL6REV infection group, indicating that anti-viral response was equally
171 triggered in monocytes in vIL6STOP and vIL6-REV infection. Nonetheless, the tSNE visualization

172 revealed that the phenotype of three immune cell populations corresponding to $CD4^+CD3^+$,
173 $CD19^+CD20^-$, and $CD123^+CD14^+$ clusters as indicated in Fig. 2B was different between infected groups
174 and mock-infected control group. The $CD123^+CD14^+$ cluster contains a heterogenous cellular population
175 that also expresses CD11c, CD16, and HLA-DR (Fig. 2A). Given that scRNA-seq results showed
176 preferential KSHV infection in $CD14^+$ cell population in association with *CD123* (IL3R) upregulation
177 (Fig. 1C), we considered that the changes observed in $CD123^+CD14^+$ cluster represent host cell anti-
178 virus response in monocytes after KSHV infection. Changes in $CD4^+CD3^+$, $CD19^+CD20^-$ clusters could
179 be the result of infection and/or indirect activation such as through cytokine production from PBMC in
180 response to KSHV infection.

181 To evaluate signaling events in detail, we next used a knowledge-based analysis and identified
182 25 immune cell subsets based on the gating described in SFig.2. The activation status of each signaling
183 molecule was evaluated among plasmacytoid dendritic cells (pDC) and monocytic cell subsets including
184 $CD123^+CD11c^+$ cells, myeloid (m)DC, $CD14^{lo}CD16^+$ non-classical monocytes, $CD14^+CD16^+$
185 intermediate monocytes, and $CD14^-CD16^+$ classical monocytes (SFig.2), based on the fold change in the
186 CyTOF signal intensity for infected groups compared to mock-infected (PBS) control group (Fig. 2C
187 and D). As expected, many of the 10 signaling molecules including STAT1, IKB, and phosphor-PLCγ
188 were strongly upregulated in pDC (Fig. 2C), an immune cell subset responsible for the anti-viral
189 response. Among $CD11c^+$ DC subsets, STAT1 and phospho-STAT3 were the two most significantly
190 activated pathways in $CD123^+CD11c^+$ cells, and less so in myeloid (m)DC (Fig. 2C and D). Among
191 monocyte subsets, STAT1, phospho-STAT3, and pS6 were upregulated after infection (Fig. 2C and D).
192 Consistent with the tSNE, the activation profiles of 10 signaling molecules in pDC, DC, and monocytes
193 were identical between vIL6STOP and vIL6REV infection (Fig. 2C and D). Thus, at 1dpi both
194 vIL6STOP and vIL6REV viruses triggered indistinguishable host responses in pDC, DCs, and
195 monocytes.

196 We also confirmed by flow cytometry approach that the frequency of $CD123^+CD11c^+$ cell
197 population among PBMC at 1dpi increased by infection regardless of the vIL6 expression (Fig. 2E and
198 F) in association with upregulation of STAT 1, pSTAT3, and pS6 (Fig. 2C and D). Notably, the
199 frequency of the $CD14^+CD16^+$ population also increased by infection in a manner dependent on the
200 KSHV vIL6 expression (Fig. 2E and F). The vIL6-dependent response suggests a biological role of vIL6
201 in the activation of infected $CD14^+CD16^+$ monocytes.
202

203 **KSHV infection promotes activation and proliferation of CD14+ monocytes in a manner**
204 **dependent on vIL-6.**
205
206 To further study the biological significance of vIL6 expression and STAT 1 and 3 activation, monocytes
207 were isolated from PBMCs (n=6) using a negative magnetic beads enrichment method and infected with
208 vIL6STOP or vIL6REV KSHV (MOI=1). The viability and frequency of immune cell subsets were then
209 analyzed by flow cytometry at 2 dpi. We found that total cell viability (Fig. 3A) and the frequency of
210 activated CD274 (PDL-1) $^{+}$ cells (Fig. 3C) were significantly increased by KSHV infection regardless of
211 the expression of vIL6. These results are expected from the CyTOF signaling analysis that demonstrates
212 that the initial host response against vIL6REV and vIL6STOP infection was indistinguishable. As shown
213 in Fig. 1, KSHV infection promptly induced inflammatory cytokine expression in monocytes.
214 Inflammatory cytokines such as TNFα produced by activated monocytes can support their survival in an
215 autocrine manner during an inflammatory response (Wolf et al., 2017). Therefore, it is possible that the
216 effect of vIL6 on cell survival, if any, could be overridden by the effect of other inflammatory cytokines
217 during the early host anti-viral response against KSHV.
218 On the other hand, the frequency of Ki67^{+} proliferating cells and that of CD16^{+}CD14^{+} cells were
219 significantly increased in a manner dependent on the presence of vIL6 (Fig. 3B and C). In monocyte
220 cultures, larger and more frequent proliferating cell blasts were observed in vIL6REV infection compared
221 to vIL6STOP infection (Fig. 3D). Intracellular staining of monocytes also confirmed that the frequency
222 of pSTAT1 and pSTAT3 in monocytes was higher in vIL6REV-infection compared to that in vIL6STOP
223 or mock-infection (Fig. 3E). These results collectively suggest that vIL6 expression during the early
224 KSHV infection increases the proliferation of infected monocytes via STAT 1 and 3 activation. The
225 cellular environment in monocytes may have a unique role in sustaining STAT activation with KSHV
226 infection.
227
228 **KSHV infection changes the transcriptional landscape of macrophages in a manner dependent on**
229 **vIL6 expression.**
230
231 To reveal the biological effect of vIL6 expression in infected monocytes, we next conducted a
232 transcriptomic analysis of *de novo* infected monocytes. To this end, total RNA was isolated from
233 monocytes harvested 7 days post KSHV infection and RNA-seq was performed (Fig. 4A in the

234 Left panel). By 7 days post-infection, the recovery of vIL6REV-infected monocytes was higher
235 than vIL6STOP-infected monocytes as shown later in Fig. 5A because of the increased Ki67^{+}
236 proliferative responses (Fig. 3B and C). Principal component analysis (PCA) demonstrated
237 remarkably distinct transcriptional profiles between vIL6REV-infected and vIL6STOP-infected
238 monocytes (Fig. 4A, the Right panel). Volcano plots show higher numbers of differentially
239 regulated genes in vIL6REV-infected monocytes (Fig. 4B). To our surprise, vIL6STOP infection
240 had little impact on the transcriptional landscape of monocytes by 7dpi, suggesting that vIL6
241 expression is needed for either sustaining cell signaling activation or maintaining KSHV lytic
242 replication. Those two functions of vIL6 are likely to be mutually exclusive.
243 Among those differentially expressed genes between vIL6REV vs vIL6STOP infection,
244 interferon-induced genes such as IFITM2, and IFITM3, are substantially upregulated in vIL6REV
245 infection (Fig.4B, Top panel). Consistently, Gene Set Enrichment Analysis (GSEA) also revealed
246 that genes associated with host anti-viral innate responses were enriched in vIL6REV infection
247 (Fig. 4C, SFig. 3), while the pathways involving in antigen processing and presentation were
248 downregulated in vIL6REV (Fig. 4D, SFig. 3). While we expected to see upregulation of IFN-
249 related genes in KSHV infected cells, down-regulation of MHC class II was unexpected.
250 Represented upregulated IFN-inducible genes and down-regulation of MHC-II were visualized in
251 the heatmap (Fig. 4E). To identify the putative transcription factors that are responsible for vIL6-
252 driven gene regulation, we examined transcription factors that are enriched on promoter regions
253 of differentially transcribed genes. As shown in Fig. 4F, interferon regulatory factors, STAT1 and
254 STAT2 were found as putative transcription factors that are responsible for driving vIL6-
255 associated phenotypes.
256
257 **KSHV infection generates macrophages with an immunosuppressive phenotype in a manner**
258 **dependent on vIL6 expression.**
259
260 Following the transcriptomic study that demonstrated transcriptional landscape changes in KSHV-
261 infected macrophages, we next confirmed functional changes induced in monocytes after KSHV *de*
262 *novo* infection on 7 dpi.
263 As shown above, in Fig. 1D, an M2-like macrophage differentiation program had been
264 triggered by 4 dpi. Consistent with this, monocytes in cultures were predominantly of large cellularity

265 with higher FSC and SSC as shown in Fig. 5A, indicative of macrophages. Also, the recovery of cells
266 at 7 dpi was significantly increased in vIL6-REV infection compared to vIL6-STOP infection.
267 Consistent with transcriptomic analysis in Fig. 4D, those macrophages derived from vIL6-REV
268 infection (vIL6-REV Mac) expressed lower levels of HLA-DR compared to control groups (Fig. 5B).
269 To test the direct effect of vIL6 in such phenotypic changes, we generated functional recombinant vIL6
270 capable of activating STAT1 (SFig. 1B and C). Monocytes were cultured in the presence of vIL6 (200
271 ng/ml in serum-free medium) for 7 days, and the phenotype was analyzed by flow cytometry. As
272 shown in Fig. 5C, the overall monocyte viability was increased from 20% to 59% in the presence of
273 vIL6. In addition, monocytes recovered from the 7 days culture showed reduced HLA-DR expression
274 (Fig. 5D) compared to monocytes cultured without vIL6. The results suggested that vIL6 treatment
275 alone could induce phenotypic changes similar to vIL6REV infection.
276 Finally, to evaluate T cell co-stimulatory capacity, CSFE-labeled allogeneic T cells were
277 cultured with macrophages derived from monocytes mock-infected or infected with vIL6REV or
278 vIL6STOP. T cell proliferation was then evaluated as CSFE-dilution by flow cytometry (Fig. 5E, Top
279 panel) in the presence or absence of anti-CD3 stimulation, and with the T cell culture with anti-
280 CD3/CD28 tetramer stimulation as a positive control. As shown in Fig. 5E and summarized in Fig. 5F,
281 the frequency of CFSE-negative proliferated T cells was significantly reduced in co-culture with
282 macrophages from vIL6REV infection (18.5%) compared with uninfected (50.8%) or vIL6STOP-
283 infection groups (78.6%) in the presence of anti-CD3 stimulation. Similar results were found in the
284 cultures without anti-CD3 stimulation except for the extent of T cell proliferation was smaller. These
285 observations are consistent with the transcriptional analysis in Fig. 4, which collectively demonstrates
286 that sustained vIL6-driven KSHV-lytic infection and continuous host anti-viral response in infected
287 monocytes induces immune suppressive phenotype in differentiating macrophages.
288 Monocytes play a key role in early infections by producing inflammatory cytokines and
289 differentiating into subtypes that play distinct roles in the induction or resolution of inflammation
290 (Watanabe et al., 2019) (Kapellos et al., 2019). Upon activation, some monocytes upregulate CD16
291 (FcgRIII), giving rise to $CD14^{+}CD16^{+}$ intermediate monocytes and $CD14^{-}CD16^{+}$ non-classical
292 monocytes, with a prolonged circulating lifespan. These $CD16^{+}$ monocytes normally exhibit high HLA-
293 DR expression for the capability of antigen presentation, transendothelial migration, and FcR-mediated
294 phagocytosis for anti-viral response (Yeap et al., 2016). $CD16^{+}$ monocytes also express the highest levels
295 of TNFR2 (CD120b) (Hijdra et al., 2012), which can upregulate anti-inflammatory IL-10 cytokine (Gane

296 et al., 2016) and supports either cell survival or death (Webster and Vucic, 2020). In this context, we
297 observed a sharp increase in $CD14^+CD16^+$ cells during early *de novo* KSHV infection (Fig.2E). We
298 speculate that KSHV infects $CD14^+CD16^+$ monocytes by exploiting their FcR- and complement-
299 mediated phagocytosis mechanism. The vIL6-driven sustained STAT1/3 activation may provide
300 infected monocytes with a proliferative advantage over uninfected cells to increase their population size.
301 Furthermore, vIL6-driven lytic infection constitutively triggers host anti-viral responses such as IFN-
302 pathway activation, which in turn, induces regulatory mechanisms (McNab et al., 2015). In the case of
303 *Mycobacterium*-infected macrophages, Type-I IFN signaling decreases energy metabolism (i.e.
304 glycolysis and mitochondrial functions) (Olson et al., 2021) and causes cell death (Zhang et al., 2021).
305 In *Listeria*-infected macrophages, stress-induced p38 mitogen-activated protein kinases (MAPK)
306 signaling synergistically enhances IFN-stimulated genes (ISGs). In macrophages, IL-10 production as a
307 part of the IFN-induced regulatory mechanism has been shown to dampen the capability of T cell
308 activation and antigen presentation (McNab et al., 2014; Redpath et al., 1999; Zdrenghea et al., 2015).
309 We show that the induction of a suppressive M2-like macrophage gene program was induced as early as
310 4 dpi in our scRNA analysis (Fig. 1). Consistent with this, earlier studies by other researchers also showed
311 that KSHV infection and STAT3 activation induce suppressive phenotype in dendritic cells and THP-1
312 cell line (Bhaskaran et al., 2017; Campbell et al., 2014; Gilardini Montani et al., 2020; Qin et al., 2010).
313 Accumulation of such immunosuppressive macrophages may increase the risk of secondary infection or
314 cause chronic infection and inflammation in the host by dysregulating immune responses; this
315 mechanism may increase the risk of KSHV-associated disease development.
316 In summary, this study demonstrates the preferential KSHV infection in monocytes and
317 highlights the critical role of vIL6 in expanding infected monocytes that facilitate a long-term virus
318 reservoir. Similar hijacking strategies to exploit monocyte development and functions have been also
319 reported in Cytomegalovirus (Baasch et al., 2021; Baasch et al., 2020; Cojohari et al., 2020; Shnayder et
320 al., 2020). The current study was unique in that vIL6STOP and vIL6REV rKSHV infection system was
321 introduced to delineate the role of vIL6 from that of the other KSHV-encoded multifunctional factors;
322 however, this study does not clarify whether vIL6 is directly involved as a driver in the expression of
323 ISGs under the host defense program in infected monocytes. Nonetheless, vIL6 was required for
324 sustaining KSHV lytic infection in monocytes, which activates IFN pathways. In lack of vIL6, KSHV
325 infection in monocytes generated macrophages indistinguishable from those from uninfected monocytes.
326 In this context, our study suggests that vIL6 and monocytes/macrophages are important therapeutic

327 targets in KSHV-associated diseases. Understanding the mechanism in which vIL6 overcomes the IFN-
328 induced regulatory mechanism and promotes cell proliferation would help develop therapies for KSHV
329 infection. It is also important to determine whether KSHV establishes latent infection in macrophages to
330 facilitate a life-long viral reservoir in patient samples. Of note, KSHV is found in circulating monocytes
331 and macrophages (Decker et al., 1996; Rappocciolo et al., 2006), and blood-derived KS-like spindle cells
332 were found to express macrophage markers (Uccini et al., 1997). Future studies are needed to investigate
333 the possible role of monocytes/macrophages as a long-term viral reservoir in patients with KSHV-
334 associated diseases.

335 **Materials and Methods**

336

337 **Cells.** LRC from healthy donor was purchased from Vitalant. PBMCs were prepared by a standard Ficoll
338 gradient method. PBMCs with a 10-30% range of $CD14^+$ monocytes content measured by flow
339 cytometry were stored in liquid N2 and used for experiments. PBMC were thawed in warm media,
340 washed twice, counted by Countess automated cell counter (ThermoFisher), and resuspended at 2-
341 $5x10^6$ viable cells/ml. Monocytes were isolated with EasySep™ Human monocyte isolation kit
342 (STEMCELL) according to the manufacturer's protocol. PBMCs and $CD14^+$ monocytes were cultured
343 in RPMI1640 medium containing 10% FBS plus antibiotics (2-5 x 10^6 cells/ml, 200uL/well in a 96 well
344 plate, 400uL/well in a 48 well plate, or 1ml/well in a 24 well plate) supplemented with or without stimuli
345 for various time as described in each figure legend.

346

347 **Virus preparation.** Doxycycline-inducible rKSHV.291 producer iSLK.291 cell lines were maintained
348 in DMEM supplemented with 10% FBS, 1% penicillin-streptomycin-L-glutamine solution, 10
349 μg/mL puromycin, 400 μg/mL hygromycin B, and 250 μg/mL G418. For virus preparation,
350 iSLK.291 cell lines were stimulated with 0.3 mM Sodium Butylate and 1 μg/ml Doxycycline for 5 days.
351 Recombinant KSHV particles were then purified after two serial ultracentrifugations from the culture
352 supernatant of activated iSLK.291 cell lines. Briefly, the culture supernatant was centrifuged at 300 ×
353 g for 10 min, and then passed through a 0.8-μm filter to remove cellular debris, and then viral
354 particles were concentrated by ultracentrifugation at 25,000 rpm for 2 hrs at 4°C with a Beckman
355 SW28 rotor. The viral precipitates were resuspended in 500 μL of DMEM along with the residual
356 ~500 μL media in the centrifuge tube and stored at −80°C until use.

357

358 **Quantification of viral copy number**. Two hundred microliters of cell culture supernatant were
359 treated with DNase I (12 μg/mL) for 15 min at room temperature to degrade unencapsidated
360 DNA. This reaction was stopped by the addition of EDTA to 5 mM followed by heating at 70°C
361 for 15 min. Viral genomic DNA was purified using the QIAamp DNA Mini Kit according to the
362 manufacturer's protocol and eluted in 100 μL of buffer AE. Four microliters of the eluate were
363 used for real-time qPCR to determine viral copy number, as described previously (Izumiya et al.,
364 2009).

365

366 **Recombinant KSHV**. To test the role of vIL6, rKSHV.291 lacking vIL6 protein expression
367 (vIL6STOP) was generated by adding stop codons in vIL6 with BAC16 (vIL6STOP). We also generated
368 a revertant rKSHV.291 with vIL6 protein expression (vIL6REV) by changing the sequence of
369 vIL6STOP back to the original wildtype sequence with BAC-recombination.
370
371 **KSHV *de novo* infection.** KSHV infection was conducted at MOI=1. Briefly, PBMC or monocytes (1-
372 5 x 10^6 cells) were suspended in RPMI 1640 medium containing 10% FBS supplemented with 8 ug/ml
373 polybrene, and the appropriate amount of rKSHV.291 in PBS (less than 10% of total volume) or PBS
374 alone as the mock infection was added to the culture. Cells were kept in the same culture medium until
375 analysis.
376
377 **Single-cell RNA-seq.** 2 x 10^6 PBMC were infected with rKSHV.291 at MOI=1, washed and fixed with
378 paraformaldehyde according to the 10X genomics cell preparation guide (CG000053) at various time
379 points (day 0, 1, 2, and 4) after infection. Single-cell suspensions (10^4 cells) were loaded to the chips
380 and subjected to the Chromium Controller (10x Genomics) to generate single-cell gel beads in
381 emulsion according to the manufacturer's protocols, and the library was constructed using
382 Chromium Single Cell 3' Reagent Kits v2 (10x Genomics). Libraries were multiplex sequenced
383 (2 × 150bp, paired-end, ~50 million mapped reads/mate pairs per sample) on an Illumina Hiseq
384 4000 sequencing system. Single-cell data were analyzed with the Cell Ranger v2.1 pipeline (10x
385 Genomics). The pipeline included alignment to the hg38 human reference genome and human
386 herpesvirus 8 strain (GQ994935.1) reference genome, Uniform Manifold Approximation and
387 Projection (UMAP), and K-means clustering. Read count matrices obtained from the pipeline were
388 normalized using the log normalization method with the "Seurat" R package (Stuart et al., 2019).
389 We investigated the association between genes using the Pearson product-moment correlation
390 coefficient. To compute the correlation coefficient and p-value, we utilized the cor.test() function
391 from the stats package in R (R. Core Team, 2021).
392
393 **Total RNA-seq.** RNA was prepared from infected monocytes using a QIAGEN miniprep kit
394 according to the manufacturer's protocol. Indexed, stranded mRNA-seq libraries were prepared
395 from total RNA (100 ng) using the KAPA Stranded mRNA-Seq kit (Roche) according to the
396 manufacturer's standard protocol. Libraries were pooled and multiplex sequenced on an Illumina

397 NovaSeq 6000 System (150-bp, paired-end, >30 × 10^6 reads per sample). RNA-Seq data was
398 analyzed using a Salmon-tximport-DESeq2 pipeline. Raw sequence reads (FASTQ format) were
399 mapped to the reference human genome assembly (GRCh38/hg38, GENCODE release 36) and
400 quantified with Salmon (Patro et al., 2017). Gene-level counts were imported with *tximport*
401 (Soneson et al., 2015). The resulting data were first filtered by average normalized count data >1
402 and differential expression analysis was performed with the software Subio Platform ver.1.24
403 (Subio Inc., Amami, Japan). For transcription factor analysis, differential expressed genes were
404 submitted to Chip-Atlas to analyze common regulators and to predict transcription factor binding
405 (Oki et al., 2018).
406
407 **Phosphoflow PBMC CyTOF:** This assay was performed by the Human Immune Monitoring
408 Center at Stanford University. PBMC were infected with rKSHV.291, washed twice with PBS and
409 then fixed with paraformaldehyde. Cells were washed twice with CyFACS buffer (PBS
410 supplemented with 2% BSA, 2 mM EDTA, and 0.1% sodium azide) and stained for 30 min at
411 room temperature with 20 mL of surface antibody cocktail. Cells were washed twice with
412 CyFACS, permeabilized with 100% methanol, and kept at -80C overnight. The next day, cells
413 were washed with CyFACS buffer and resuspended in a 20 mL intracellular antibody cocktail in
414 CyFACS for 30 min at room temperature before washing twice in CyFACS. Cells were
415 resuspended in a 100 mL iridium-containing DNA intercalator (1:2000 dilution in 2% PFA in
416 PBS) and incubated at room temperature for 20 min. Cells were washed once with CyFACS buffer
417 and twice with MilliQ water. Cells were diluted to 750x10^5 cells/mL in MilliQ water and acquired
418 on CyTOF. Data analysis was performed using FlowJo v10.8.1 by gating on intact cells based on
419 the iridium isotopes from the intercalator, then on singlets by Ir191 vs cell length followed by cell
420 subset-specific gating as described in SFig. 2.

421 **Flow cytometry.** Cells in culture were washed twice with PBS and resuspended in FACS buffer
422 (PBS supplemented with 1% FBS) at 1x10^7 cells/ml. 50 uL cells per well were stained with Aqua
423 LIVE/DEAD cell viability dye (Invitrogen, Carlsbad, CA) according to the manufacturer's
424 instructions, washed with FACS Buffer, and then stained for 45 min at room temperature with the
425 antibodies shown in the table. For intracellular staining of pSTAT1 and pSTAT3, cells were fixed
426 with paraformaldehyde, permeabilized with methanol, and kept at -80C overnight. The cells were
427 washed with FACS buffer and stained with pSTAT-1 AlexaFluor647 and pSTAT-3

428 AlexaFluor647. Cells were washed three times with FACS buffer and resuspended in 200 uL
429 FACS buffer. For typical experiments, 1-2 x10^5 PBMC per sample were collected using DIVA 6.0
430 software on a Fortessa flow cytometer (BD Biosciences) at Flow Cytometry Shared Resource, UC
431 Davis Comprehensive Cancer Center Shared Resources. Data analysis was performed using
432 FlowJo v10.8.1 by gating on live cells based on forward versus side scatter profiles, then on
433 singlets using forward scatter area versus height, followed by dead cell exclusion using Aqua
434 LIVE/DEAD viability dye, and then cell subset-specific gating.
435
436 **T cell proliferation assay.** Monocytes were infected with vIL6REV or vIL6STOP, or mock-infected
437 (PBS). Macrophages derived from KSHV-infected monocyte cultures were recovered at 7 dpi after being
438 washed with PBS twice followed by gentle pipetting and suspended in RPMI1640 medium containing
439 10% FBS. T cells were isolated from PBMC using EasySep™ Human CD3 positive selection kit II
440 (STEMCELL) according to the manufacturer's protocol. T cells were stained in PBS with CellTrace™
441 CFSE Cell Proliferation Kit (ThermoFisher) according to the manufacturer's protocol and suspended in
442 RPMI1640 medium containing 10% FBS. 10^5 CSFE-labeled CD3+ T cells were incubated with 10^4
443 macrophages from KSHV-infected monocyte cultures in 200 uL/well in a 96-well U-bottom plate,
444 without or with 100 ng/ml anti-CD3 antibody (BD Bioscience) for 5 days. For positive and negative
445 controls, T cells were stimulated with ImmunoCult Human CD3/28 T cell activator or left unstimulated.
446 Cells were recovered from cultures and analyzed by BD Accuri™ flow cytometer. 10^4 events were
447 acquired for each sample. Data analysis was performed using FlowJo v10.8.1 by gating
448 lymphocytes based on forward versus side scatter profiles. The average frequencies of the CFSE-
449 negative population were determined based on the negative control.
450
451 **Statistical analysis.** Whenever applicable, experimental replicates of at least 3 for each sample
452 including negative controls were prepared. Results are shown as mean ± SD from at least three
453 independent experiments. Statistical analyses were performed using GraphPad Prism 9.4.1 software.
454 Statistical significance was determined by appropriate testing, Student's t-test, one-way ANOVA with
455 Tukey's multiple comparison test, and correction for false discovery rate (FDR). A value of $p < 0.05$
456 was considered statistically significant.
457
458

459 **Online supplemental material**

460 The supplemental material includes characterization and validation of recombinant vIL6STOP and
461 vIL6REV KSHV and recombinant vIL6 used in this study (SFig.1), a gating strategy of immune
462 cells for CyTOF analysis (SFig. 2), and GSEA analysis of RNAseq data comparing vIL6REV-
463 infected and uninfected macrophages (SFig. 3).

464

465 **Data availability**

466 The data underlying Figs. 1, 2, and 4 are openly available in [XXX] at [XXX]. The data
467 underlying Figs. 2, 3, and 5 are available in the published article and its online supplemental
468 material.

469

470 **Acknowledgment**

471 The authors would like to thank Dr. Robert Yarchoan (National Cancer Institute, USA) and Dr.
472 Harutaka Katano (National Institute of Infectious Disease, Japan) for the generous gift of rabbit
473 monoclonal antibodies against vIL6. We would like to thank Andreas Koni for his assistance in
474 preparing the manuscript. We would like to thank Immune Modeling, Analysis and Diagnostic,
475 Genomics, and Flow Cytometry UC Davis Comprehensive Cancer Center Shared Resources for
476 expert support with 10X scRNA-seq, total RNA-Seq, and flow cytometry analyses and Stanford
477 Human Immune Monitoring Center for expert CyTOF analysis.

478

479 This work was supported by grants from the National Cancer Institute CA232845-02S1 (M.
480 Shimoda), CA225266, CA232845, and AI167663 (Y. Izumiya), and UC Davis Dermatology
481 Seed grant (M. Shimoda). M. Shimoda was supported by the National Cancer
482 Institute/CRCHD/CURE program. The Immune Modeling, Analysis and Diagnostic, Genomics,
483 and Flow Cytometry Shared Resources are supported by the UC Davis Comprehensive Cancer
484 Center Support Grant (CCSG) awarded by the National Cancer Institute (NCI P30CA093373).

485

486 **Author contributions**

487 Conceptualization: M. Shimoda, and Y. Izumiya. Experimental design: M. Shimoda and Y.
488 Izumiya. Experiment and Data acquisition and analysis: M. Shimoda, R. Davis, A. Merleev, T.
489 Inagaki, and Y. Izumiya. Funding acquisition: M. Shimoda and Y. Izumiya. Manuscript

preparation: M. Shimoda. Review & Editing: M. Shimoda, R. Davis, A. Merleev, C. Tepper, E. Maverakis, T. Inagaki, and Y. Izumiya.

495 Figure 1. KSHV preferentially infects monocytes and triggers the monocyte inflammatory
496 transcription program. PBMCs were infected with rKSHV.291 at MOI=1, fixed at various time points
497 (pre-infection, day 1, 2, and 4) after infection, and subjected to 10X scRNA-seq analysis. (A) UMAP
498 visualizes 9 PBMC clusters in a preinfectional sample based on lineage-specific gene expression of
499 *KLRD1, CD14, APOBEC3A, VMO1, CD79A*, and *CD3E* genes for NK cells, monocytes, intermediate
500 monocytes, non-classical monocytes, B cells, and T cells, respectively. (B) KSHV-encoded K2 (vIL6)
501 expression overlapped with CD14 expression at 1 dpi. (C) The kinetic scRNA-seq analysis on pre-
502 infection, 1 dpi, 2 dpi, and 4 dpi revealed that KSHV infection in $CD14^+$ monocytes triggered the
503 activation and inflammatory response with the upregulation of *IL3RA* (CD123), *CCL2*, and *TNFα*. (D)
504 Expression of genes in $CD14^+$ monocytes associated with differentiation of M2-like macrophages with
505 suppressive phenotype (*CD274/PD-L1*, *C1QA*, *RNASE1*, *IL-10*, and *CD163*). Gene expression levels
506 are indicated by heatmap bars. A representative result of three experiments is shown.
507
508 Figure 2. KSHV infection preferentially triggers STAT activation in monocytes and dendritic
509 cells. PBMC from healthy donors (n=6, 3 males and 3 females) were infected with vIL6REV (with
510 vIL6 expression) or vIL6STOP (without vIL6 expression) (MOI=1), or mock-infected (PBS). At 1
511 dpi, cells were fixed and subjected to CyTOF analysis. The expression levels of 10 signaling molecules
512 were evaluated. (A) tSNE for dimension reduction analysis was applied for each infection group after
513 1000 events from 6 samples in each group were concatenated. Immune cell subsets were clustered
514 based on each marker expression (Right panel). (B) The phenotypic changes induced in three immune
515 cell populations corresponding to $CD4^+CD3^+$, $CD19^+CD20^-$, and $CD123^+CD14^+$ clusters by infection
516 were identified by comparison between vIL6STOP, vIL-6REV, and mock-infected (PBS) control
517 group. (C) The activation status of 10 signaling molecules among plasmacytoid dendritic cells (pDC)
518 and monocytic cell subsets including $CD123^+CD11c^+$ cells, myeloid (m)DC, $CD14^{lo}CD16^+$ non-
519 classical monocytes, $CD14^+CD16^+$ intermediate monocytes, and $CD14^-CD16^+$ classical monocytes are
520 shown in heat maps. Each subset was identified based on the lineage cell surface marker expression
521 with gating strategies shown in SFig.2. (D) The fold change in the CyTOF signal intensity of STAT1
522 and pSTAT3 for $CD123^+CD11c^+$ cells (TOP panel) and $CD14^+CD16^+$ cells (Bottom panel) in infected
523 groups compared to mock-infected (PBS) control group are shown. (E) Representative FACS profiles
524 of infected PBMC were analyzed by flow cytometry at 1 dpi. The frequency of $CD123^+CD11c^+$ (Top)
525 and $CD14^+CD16^+$ (Bottom) cell population in a live CD3-CD56-CD19- HLA-DR+ cell gate is shown

526 with the percentages. (F) Individual percentages of $CD123^{+}CD11c^{+}$ and $CD14^{+}CD16^{+}$ cells in (E) for
527 each PBMC sample (n=6) are compared between vIL6REV- and vIL6STOP- infected groups, and
528 uninfected group (PBS). p values shown are by one-way ANOVA with Tukey's multiple comparison
529 test. $p<0.05$: statistically significant.
530
531 Figure 3. KSHV preferentially infects and expands CD14+ monocytes with an inflammatory response
532 in a manner dependent on vIL6. Monocytes were isolated negatively from PBMCs (n=6) using
533 magnetic beads and infected with vIL6STOP or vIL6REV rKSHV (MOI=1). (A) The frequencies of
534 live cells on 2 dpi by live/dead staining are shown (B) Representative FACS profiles of infected
535 monocytes analyzed by flow cytometry for Ki67, CD16, and PD-L1 expressing cells. (C) The
536 frequencies for Ki67+, CD16+, and PDL-1+ cells are shown. (D) Representative images of cell blasts
537 in indicated treatment (x100). (E) Representative FACS profiles of each sample for pSTAT1 and
538 pSTAT3 intracellular staining with the percentage of gated pSTAT1- and pSTAT3- expressing cells
539 are shown. *p* values shown are by ANOVA with a paired comparison with Tukey's multiple
540 comparison test. $p < 0.05$: statistically significant.
541
542
543 Figure 4. Differential expression genes analysis between wild-type KSHV and vIL6 deficient
544 KSHV infected monocytes. (A) A schematic illustration of the KSHV infection experiment
545 (Left). Monocytes were infected with vIL6REV, vIL6STOP, or mock-infected (PBS). At 7 dpi,
546 cells were harvested for RNA-seq analysis (n=2/group). Principal component analysis (PCA) of
547 RNA-seq data from independent biological replicates is shown (Right). The number in
548 parenthesis indicates the percentage of total variance explained by each PC. Colored dots
549 represent individual samples infected with mock (PBS-treated), vIL6REV, and vIL6STOP. (B)
550 Volcano plots for differentially expressed genes (log2 FC threshold = 1, *p*-value threshold =
551 0.05) between vIL6REV and vIL6STOP (Top), vIL6 REV and mock (Middle) and vIL6STOP
552 and mock (Bottom). The log2 FC indicates the mean expression for each. The functional
553 enrichment analysis of upregulated genes (C) and downregulated genes (D) in vIL6REV-
554 compared to vIL6STOP-infected monocytes. DAVID functional enrichment analysis was
555 performed, and the analysis results of the top 5 enriched pathways are shown (Right). The
556 representative results of Gene Set Enrichment Analysis (GSEA) are shown (Left). (E) Heatmap

557 of representative genes enriched for upregulated (C) or downregulated (D) in vIL6REV-
558 compared to vIL6STOP-infected monocytes. (F) Putative transcription factors that are
559 responsible for differentially expressed genes between vIL-6 REV and vIL-6 STOP KSHV
560 infection. The bar charts indicate *p* values for enrichment. The following parameters were used;
561 Organism: Homo sapiens (hg38), Experiment type: ChiP (TFs and others), Cell type Class:
562 Blood, and Threshold for significance: 50.
563
564 Figure 5. KSHV infection promotes macrophage differentiation with an immunosuppressive phenotype
565 in a manner dependent on vIL6 expression. Monocytes were infected with vIL6REV or vIL6STOP
566 (MOI=1), uninfected (PBS), or treated with vIL6 (200 ng/ml in serum-free medium) and cultured for 7
567 days. Each sample was analyzed by flow cytometry with each FMO staining as a control. (A) The
568 average frequency of macrophages in each culture (n=3) is based on representative FSC-A and SSC-A
569 profiles. (B) The average geometric mean fluorescent intensity (gMFI) of HLA-DR for each macrophage
570 sample in (A) with representative histogram overlays are shown. (C) Representative FACS plots of live
571 monocytes one week after vIL6 treatment and the average frequencies (n=3) are shown. (D) The average
572 gMFI of HLA-DR for each macrophage sample in (C) with representative histogram overlays are shown.
573 (E) An experimental design of T cell proliferation assay with macrophages (Top) and representative
574 histograms of T cells (gated based on FSC-A and SSC-A) for CSFE are shown. T cells without or with
575 anti-CD3/CD28 tetramer stimulation are used as controls. (F) The average frequencies of the CFSE-
576 negative population determined as in (E) for each sample are shown (n=3). *p* values shown are by
577 ANOVA with a paired comparison with Tukey's multiple comparison test. $p < 0.05$: statistically
578 significant.
579
580

581 **References**

582 Alomari, N., and J. Totonchy. 2020. Cytokine-Targeted Therapeutics for KSHV-Associated
583 Disease. *Viruses* 12:
584 Aoki, Y., R. Yarchoan, K. Wyvill, S. Okamoto, R.F. Little, and G. Tosato. 2001. Detection of
585 viral interleukin-6 in Kaposi sarcoma-associated herpesvirus-linked disorders. *Blood*
586 97:2173-2176.
587 Baasch, S., P. Giansanti, J. Kolter, A. Riedl, A.J. Forde, S. Runge, S. Zenke, R. Elling, A.
588 Halenius, S. Brabletz, H. Hengel, B. Kuster, T. Brabletz, L. Cicin-Sain, R. Arens, A.
589 Vlachos, J.C. Rohr, M.P. Stemmler, M. Kopf, Z. Ruzsics, and P. Henneke. 2021.
590 Cytomegalovirus subverts macrophage identity. *Cell* 184:3774-3793 e3725.
591 Baasch, S., Z. Ruzsics, and P. Henneke. 2020. Cytomegaloviruses and Macrophages-Friends and
592 Foes From Early on? *Front Immunol* 11:793.
593 Bhaskaran, N., S.K. Ghosh, X. Yu, S. Qin, A. Weinberg, P. Pandiyan, and F. Ye. 2017. Kaposi's
594 sarcoma-associated herpesvirus infection promotes differentiation and polarization of
595 monocytes into tumor-associated macrophages. *Cell Cycle* 16:1611-1621.
596 Campbell, D.M., G. Rappocciolo, F.J. Jenkins, and C.R. Rinaldo. 2014. Dendritic cells: key
597 players in human herpesvirus 8 infection and pathogenesis. *Front Microbiol* 5:452.
598 Caro-Vegas, C., S. Sellers, K.M. Host, J. Seltzer, J. Landis, W.A. Fischer, 2nd, B. Damania, and
599 D.P. Dittmer. 2020. Runaway Kaposi Sarcoma-associated herpesvirus replication
600 correlates with systemic IL-10 levels. *Virology* 539:18-25.
601 Cesarman, E., B. Damania, S.E. Krown, J. Martin, M. Bower, and D. Whitby. 2019. Kaposi
602 sarcoma. *Nat Rev Dis Primers* 5:9.
603 Chandriani, S., and D. Ganem. 2010. Array-based transcript profiling and limiting-dilution
604 reverse transcription-PCR analysis identify additional latent genes in Kaposi's sarcoma-
605 associated herpesvirus. *J Virol* 84:5565-5573.
606 Cojohari, O., J. Mahmud, A.M. Altman, M.A. Peppenelli, M.J. Miller, and G.C. Chan. 2020.
607 Human Cytomegalovirus Mediates Unique Monocyte-to-Macrophage Differentiation
608 through the PI3K/SHIP1/Akt Signaling Network. *Viruses* 12:
609 Decker, L.L., P. Shankar, G. Khan, R.B. Freeman, B.J. Dezube, J. Lieberman, and D.A. Thorley-
610 Lawson. 1996. The Kaposi sarcoma-associated herpesvirus (KSHV) is present as an
611 intact latent genome in KS tissue but replicates in the peripheral blood mononuclear cells
612 of KS patients. *J Exp Med* 184:283-288.
613 Dittmer, D.P., and B. Damania. 2019. Kaposi's Sarcoma-Associated Herpesvirus (KSHV)-
614 Associated Disease in the AIDS Patient: An Update. *Cancer Treat Res* 177:63-80.
615 Dumic, I., M. Radovanovic, O. Igandan, I. Savic, C.W. Nordstrom, D. Jevtic, A. Subramanian,
616 and P. Ramanan. 2020. A Fatal Case of Kaposi Sarcoma Immune Reconstitution
617 Syndrome (KS-IRIS) Complicated by Kaposi Sarcoma Inflammatory Cytokine Syndrome
618 (KICS) or Multicentric Castleman Disease (MCD): A Case Report and Review. *Am J*
619 *Case Rep* 21:e926433.
620 Fullwood, R.A., G.M. Low, E.P. Chase, M. Grasley, S.S. Beal, I.M. McCrary, C.W. Daniels, K.
621 Ingersoll, and B.K. Berges. 2018. The Kaposi's sarcoma-associated herpesvirus viral
622 interleukin 6 gene affects metastasis and expression of B cell markers in a murine
623 xenograft model. *PLoS One* 13:e0204947.
624 Gane, J.M., R.A. Stockley, and E. Sapey. 2016. TNF-alpha Autocrine Feedback Loops in Human
625 Monocytes: The Pro- and Anti-Inflammatory Roles of the TNF-alpha Receptors Support
626 the Concept of Selective TNFR1 Blockade In Vivo. *J Immunol Res* 2016:1079851.

627 Giffin, L., J.A. West, and B. Damania. 2015. Kaposi's Sarcoma-Associated Herpesvirus
628 Interleukin-6 Modulates Endothelial Cell Movement by Upregulating Cellular Genes
629 Involved in Migration. *mBio* 6:e01499-01415.
630 Gilardini Montani, M.S., L. Falcinelli, R. Santarelli, M. Granato, M.A. Romeo, N. Cecere, R.
631 Gonnella, G. D'Orazi, A. Faggioni, and M. Cirone. 2020. KSHV infection skews
632 macrophage polarisation towards M2-like/TAM and activates Ire1 alpha-XBP1 axis up-
633 regulating pro-tumorigenic cytokine release and PD-L1 expression. *Br J Cancer* 123:298-
634 306.
635 Goncalves, P.H., J. Ziegelbauer, T.S. Uldrick, and R. Yarchoan. 2017. Kaposi sarcoma
636 herpesvirus-associated cancers and related diseases. *Curr Opin HIV AIDS* 12:47-56.
637 Gregory, S.M., L. Wang, J.A. West, D.P. Dittmer, and B. Damania. 2012. Latent Kaposi's
638 sarcoma-associated herpesvirus infection of monocytes downregulates expression of
639 adaptive immune response costimulatory receptors and proinflammatory cytokines. *J*
640 *Virol* 86:3916-3923.
641 Hijdra, D., A.D. Vorselaars, J.C. Grutters, A.M. Claessen, and G.T. Rijkers. 2012. Differential
642 expression of TNFR1 (CD120a) and TNFR2 (CD120b) on subpopulations of human
643 monocytes. *J Inflamm (Lond)* 9:38.
644 Hoenen, T., and A. Groseth. 2022. Virus-Host Cell Interactions. *Cells* 11:
645 Kapellos, T.S., L. Bonaguro, I. Gemund, N. Reusch, A. Saglam, E.R. Hinkley, and J.L. Schultze.
646 2019. Human Monocyte Subsets and Phenotypes in Major Chronic Inflammatory
647 Diseases. *Front Immunol* 10:2035.
648 McNab, F., K. Mayer-Barber, A. Sher, A. Wack, and A. O'Garra. 2015. Type I interferons in
649 infectious disease. *Nat Rev Immunol* 15:87-103.
650 McNab, F.W., J. Ewbank, A. Howes, L. Moreira-Teixeira, A. Martirosyan, N. Ghilardi, M.
651 Saraiva, and A. O'Garra. 2014. Type I IFN induces IL-10 production in an IL-27-
652 independent manner and blocks responsiveness to IFN-gamma for production of IL-12
653 and bacterial killing in Mycobacterium tuberculosis-infected macrophages. *J Immunol*
654 193:3600-3612.
655 Molden, J., Y. Chang, Y. You, P.S. Moore, and M.A. Goldsmith. 1997. A Kaposi's sarcoma-
656 associated herpesvirus-encoded cytokine homolog (vIL-6) activates signaling through the
657 shared gp130 receptor subunit. *J Biol Chem* 272:19625-19631.
658 Morris, V.A., A.S. Punjabi, and M. Lagunoff. 2008. Activation of Akt through gp130 receptor
659 signaling is required for Kaposi's sarcoma-associated herpesvirus-induced lymphatic
660 reprogramming of endothelial cells. *J Virol* 82:8771-8779.
661 Morris, V.A., A.S. Punjabi, R.C. Wells, C.J. Wittkopp, R. Vart, and M. Lagunoff. 2012. The
662 KSHV viral IL-6 homolog is sufficient to induce blood to lymphatic endothelial cell
663 differentiation. *Virology* 428:112-120.
664 Oki, S., T. Ohta, G. Shioi, H. Hatanaka, O. Ogasawara, Y. Okuda, H. Kawaji, R. Nakaki, J. Sese,
665 and C. Meno. 2018. ChIP-Atlas: a data-mining suite powered by full integration of public
666 ChIP-seq data. *EMBO Rep* 19:
667 Olson, G.S., T.A. Murray, A.N. Jahn, D. Mai, A.H. Diercks, E.S. Gold, and A. Aderem. 2021.
668 Type I interferon decreases macrophage energy metabolism during mycobacterial
669 infection. *Cell Rep* 35:109195.
670 Patro, R., G. Duggal, M.I. Love, R.A. Irizarry, and C. Kingsford. 2017. Salmon provides fast and
671 bias-aware quantification of transcript expression. *Nat Methods* 14:417-419.

672 Polizzotto, M.N., T.S. Uldrick, D. Hu, and R. Yarchoan. 2012. Clinical Manifestations of Kaposi
673 Sarcoma Herpesvirus Lytic Activation: Multicentric Castleman Disease (KSHV-MCD)
674 and the KSHV Inflammatory Cytokine Syndrome. *Front Microbiol* 3:73.
675 Polizzotto, M.N., T.S. Uldrick, K.M. Wyvill, K. Aleman, V. Marshall, V. Wang, D. Whitby, S.
676 Pittaluga, E.S. Jaffe, C. Millo, G. Tosato, R.F. Little, S.M. Steinberg, I. Sereti, and R.
677 Yarchoan. 2016. Clinical Features and Outcomes of Patients With Symptomatic Kaposi
678 Sarcoma Herpesvirus (KSHV)-associated Inflammation: Prospective Characterization of
679 KSHV Inflammatory Cytokine Syndrome (KICS). *Clin Infect Dis* 62:730-738.
680 Qin, Z., P. Kearney, K. Plaisance, and C.H. Parsons. 2010. Pivotal advance: Kaposi's sarcoma-
681 associated herpesvirus (KSHV)-encoded microRNA specifically induce IL-6 and IL-10
682 secretion by macrophages and monocytes. *J Leukoc Biol* 87:25-34.
683 Rappocciolo, G., F.J. Jenkins, H.R. Hensler, P. Piazza, M. Jais, L. Borowski, S.C. Watkins, and
684 C.R. Rinaldo, Jr. 2006. DC-SIGN is a receptor for human herpesvirus 8 on dendritic cells
685 and macrophages. *J Immunol* 176:1741-1749.
686 Redpath, S., A. Angulo, N.R. Gascoigne, and P. Ghazal. 1999. Murine cytomegalovirus infection
687 down-regulates MHC class II expression on macrophages by induction of IL-10. *J*
688 *Immunol* 162:6701-6707.
689 Sakakibara, S., and G. Tosato. 2011. Viral interleukin-6: role in Kaposi's sarcoma-associated
690 herpesvirus: associated malignancies. *J Interferon Cytokine Res* 31:791-801.
691 Shnayder, M., A. Nachshon, B. Rozman, B. Bernshtein, M. Lavi, N. Fein, E. Poole, S. Avdic, E.
692 Blyth, D. Gottlieb, A. Abendroth, B. Slobedman, J. Sinclair, N. Stern-Ginossar, and M.
693 Schwartz. 2020. Single cell analysis reveals human cytomegalovirus drives latently
694 infected cells towards an anergic-like monocyte state. *Elife* 9:
695 Soneson, C., M.I. Love, and M.D. Robinson. 2015. Differential analyses for RNA-seq:
696 transcript-level estimates improve gene-level inferences. *F1000Res* 4:1521.
697 Staskus, K.A., W. Zhong, K. Gebhard, B. Herndier, H. Wang, R. Renne, J. Beneke, J. Pudney,
698 D.J. Anderson, D. Ganem, and A.T. Haase. 1997. Kaposi's sarcoma-associated
699 herpesvirus gene expression in endothelial (spindle) tumor cells. *J Virol* 71:715-719.
700 Suthaus, J., C. Stuhlmann-Laeisz, V.S. Tompkins, T.R. Rosean, W. Klapper, G. Tosato, S. Janz,
701 J. Scheller, and S. Rose-John. 2012. HHV-8-encoded viral IL-6 collaborates with mouse
702 IL-6 in the development of multicentric Castleman disease in mice. *Blood* 119:5173-
703 5181.
704 Uccini, S., M.C. Sirianni, L. Vincenzi, S. Topino, A. Stoppacciaro, I. Lesnoni La Parola, M.
705 Capuano, C. Masini, D. Cerimele, M. Cella, A. Lanzavecchia, P. Allavena, A.
706 Mantovani, C.D. Baroni, and L.P. Ruco. 1997. Kaposi's sarcoma cells express the
707 macrophage-associated antigen mannose receptor and develop in peripheral blood
708 cultures of Kaposi's sarcoma patients. *Am J Pathol* 150:929-938.
709 Uhlen, M., M.J. Karlsson, W. Zhong, A. Tebani, C. Pou, J. Mikes, T. Lakshmikanth, B.
710 Forsstrom, F. Edfors, J. Odeberg, A. Mardinoglu, C. Zhang, K. von Feilitzen, J. Mulder,
711 E. Sjostedt, A. Hober, P. Oksvold, M. Zwahlen, F. Ponten, C. Lindskog, A. Sivertsson, L.
712 Fagerberg, and P. Brodin. 2019. A genome-wide transcriptomic analysis of protein-
713 coding genes in human blood cells. *Science* 366:
714 van der Meulen, E., M. Anderton, M.J. Blumenthal, and G. Schafer. 2021. Cellular Receptors
715 Involved in KSHV Infection. *Viruses* 13:
716 Watanabe, S., M. Alexander, A.V. Misharin, and G.R.S. Budinger. 2019. The role of
717 macrophages in the resolution of inflammation. *J Clin Invest* 129:2619-2628.

718 Webster, J.D., and D. Vucic. 2020. The Balance of TNF Mediated Pathways Regulates
719 Inflammatory Cell Death Signaling in Healthy and Diseased Tissues. *Front Cell Dev Biol*
720 8:365.
721 Wolf, Y., A. Shemer, M. Polonsky, M. Gross, A. Mildner, S. Yona, E. David, K.W. Kim, T.
722 Goldmann, I. Amit, M. Heikenwalder, S. Nedospasov, M. Prinz, N. Friedman, and S.
723 Jung. 2017. Autonomous TNF is critical for in vivo monocyte survival in steady state and
724 inflammation. *J Exp Med* 214:905-917.
725 Yeap, W.H., K.L. Wong, N. Shimasaki, E.C. Teo, J.K. Quek, H.X. Yong, C.P. Diong, A.
726 Bertoletti, Y.C. Linn, and S.C. Wong. 2016. CD16 is indispensable for antibody-
727 dependent cellular cytotoxicity by human monocytes. *Sci Rep* 6:34310.
728 Zdrenghea, M.T., H. Makrinioti, A. Muresan, S.L. Johnston, and L.A. Stanciu. 2015. The role of
729 macrophage IL-10/innate IFN interplay during virus-induced asthma. *Rev Med Virol*
730 25:33-49.
731 Zhang, L., X. Jiang, D. Pfau, Y. Ling, and C.F. Nathan. 2021. Type I interferon signaling
732 mediates Mycobacterium tuberculosis-induced macrophage death. *J Exp Med* 218:
733 Zhu, X., Y. Guo, S. Yao, Q. Yan, M. Xue, T. Hao, F. Zhou, J. Zhu, D. Qin, and C. Lu. 2014.
734 Synergy between Kaposi's sarcoma-associated herpesvirus (KSHV) vIL-6 and HIV-1 Nef
735 protein in promotion of angiogenesis and oncogenesis: role of the AKT signaling
736 pathway. *Oncogene* 33:1986-1996.
737

738

Figure 1

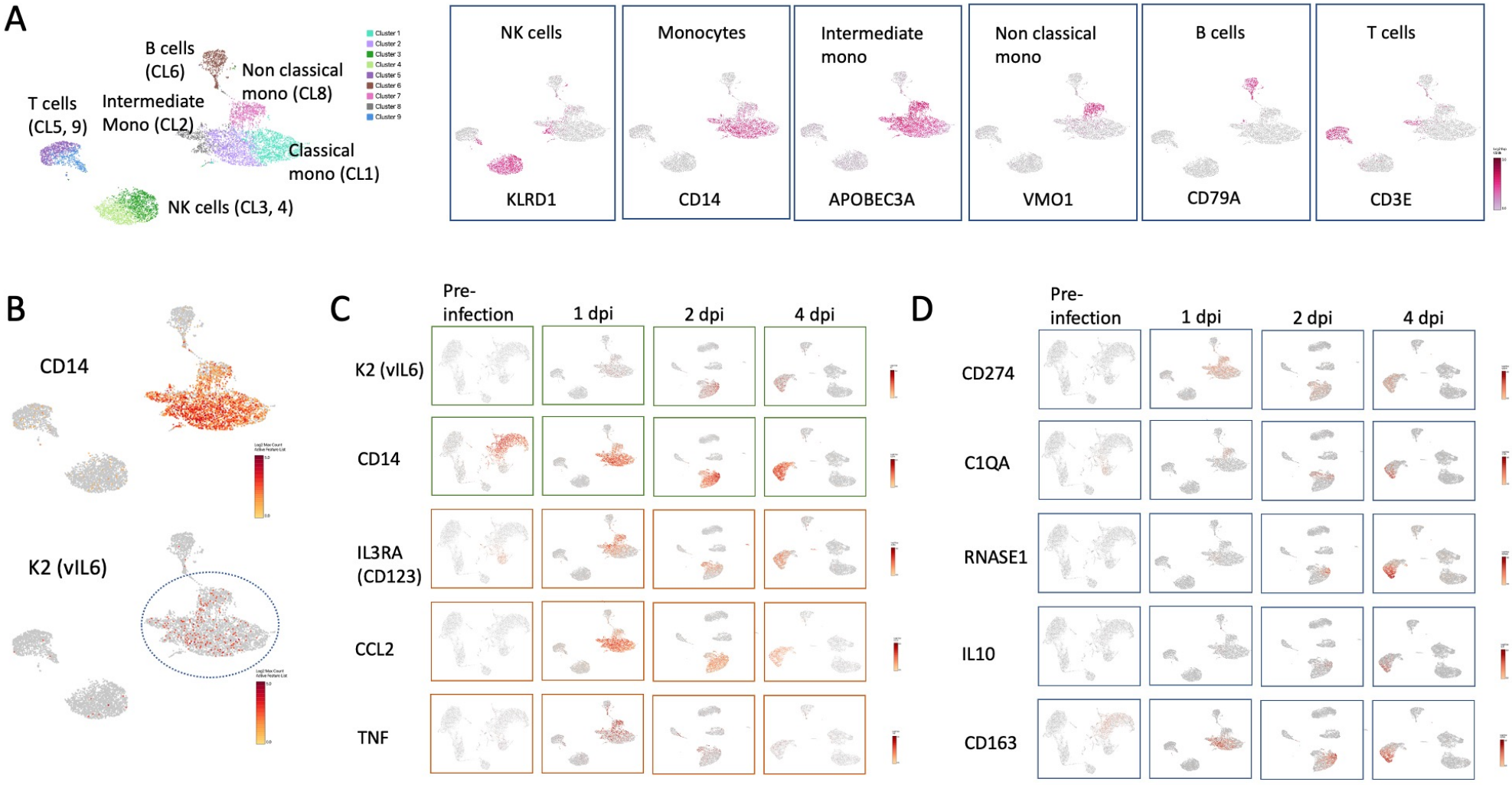
A
B cells (CL6)
Non classical mono (CL8)
T cells (CL5, 9)
Intermediate Mono (CL2)
Classical mono (CL1)
NK cells (CL3, 4)
NK cells
KLRD1
Monocytes
CD14
Intermediate mono
APOBEC3A
Non classical mono
VMO1
B cells
CD79A
T cells
CD3E
B
CD14
K2 (vIL6)
C
Pre-infection
1 dpi
2 dpi
4 dpi
K2 (vIL6)
CD14
IL3RA (CD123)
CCL2
TNF
D
Pre-infection
1 dpi
2 dpi
4 dpi
CD274
C1QA
RNASE1
IL10
CD163

Figure 2

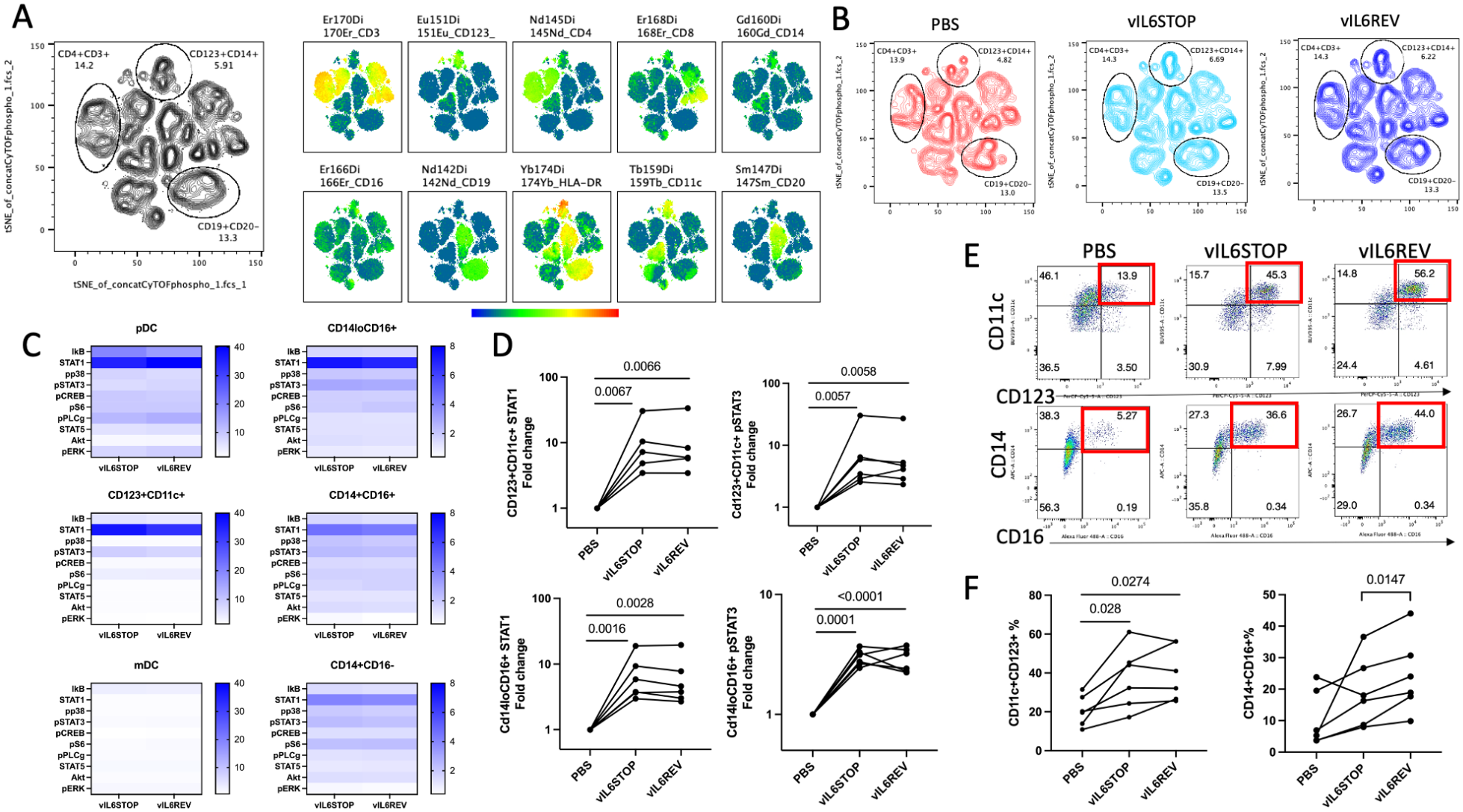
A
CD4+CD3+ 14.2
CD123+CD14+ 5.91
CD19+CD20- 13.3
tSNE_of_concatCyTOFphospho_1.fcs_1
Er170Di 170Er_CD3
Eu151Di 151Eu_CD123_
Nd145Di 145Nd_CD4
Er168Di 168Er_CD8
Gd160Di 160Gd_CD14
Er166Di 166Er_CD16
Nd142Di 142Nd_CD19
Yb174Di 174Yb_HLA-DR
Tb159Di 159Tb_CD11c
Sm147Di 147Sm_CD20
B
PBS
vIL6STOP
vIL6REV
CD4+CD3+ 13.9
CD123+CD14+ 4.82
CD19+CD20- 13.0
CD4+CD3+ 14.3
CD123+CD14+ 6.69
CD19+CD20- 13.5
CD4+CD3+ 14.3
CD123+CD14+ 6.22
CD19+CD20- 13.3
C
pDC
CD14loCD16+
CD123+CD11c+
CD14+CD16+
mDC
CD14+CD16-
IkB
STAT1
pp38
pSTAT3
pCREB
pS6
pPLCg
STAT5
Akt
pERK
vIL6STOP
vIL6REV
D
CD123+CD11c+ STAT1 Fold change
0.0066
0.0067
Cd123+CD11c+ pSTAT3 Fold change
0.0058
0.0057
Cd14loCD16+ STAT1 Fold change
0.0028
0.0016
Cd14loCD16+ pSTAT3 Fold change
<0.0001
0.0001
PBS
vIL6STOP
vIL6REV
E
PBS
vIL6STOP
vIL6REV
CD11c
CD123
CD14
CD16
46.1
13.9
36.5
3.50
15.7
45.3
30.9
7.99
14.8
56.2
24.4
4.61
38.3
5.27
56.3
0.19
27.3
36.6
35.8
0.34
26.7
44.0
29.0
0.34
F
CD11c+CD123+ %
0.0274
0.028
CD14+CD16+%
0.0147
PBS
vIL6STOP
vIL6REV

Figure 3

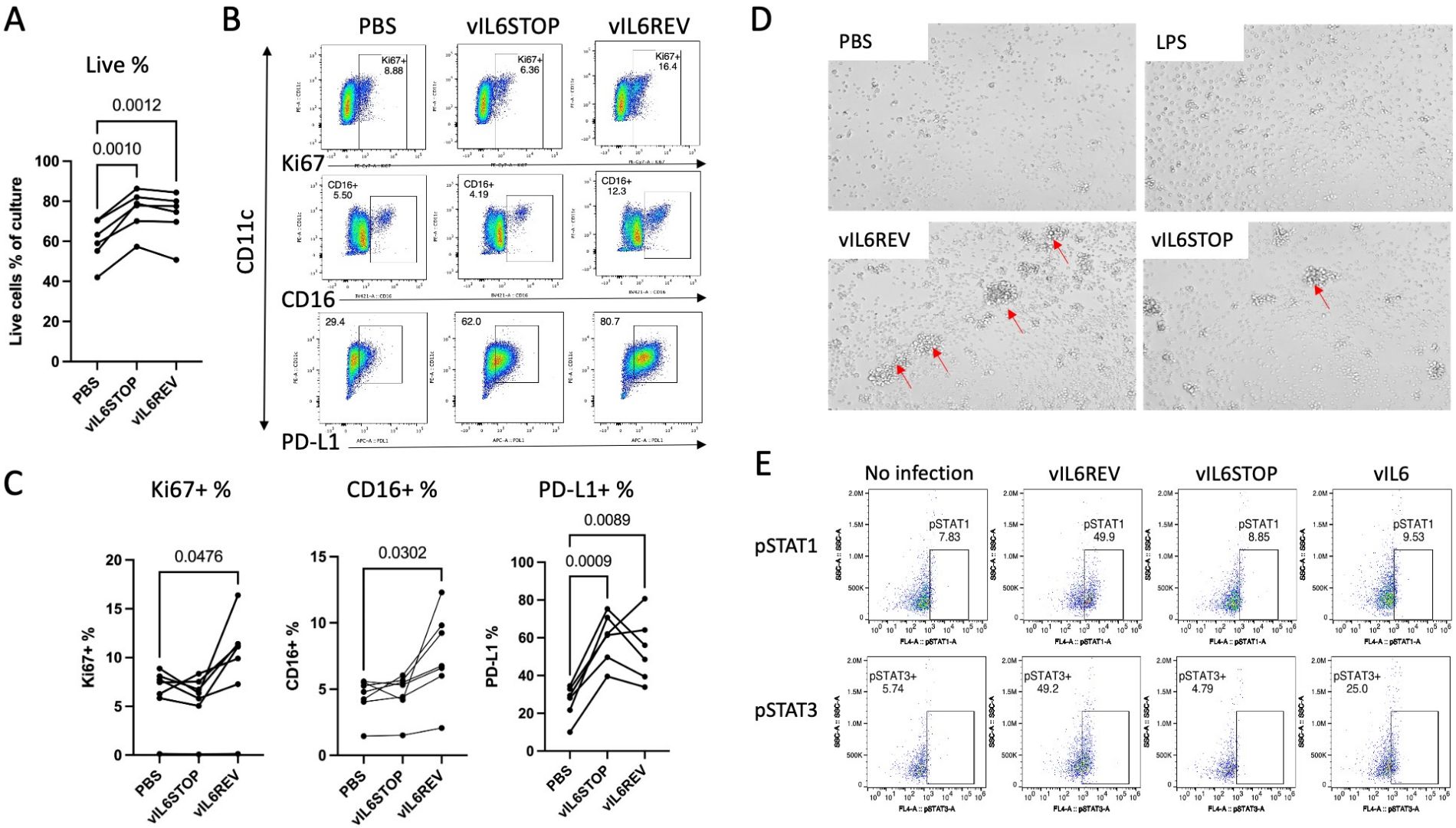
A
Live %
0.0012
0.0010
Live cells % of culture
PBS
vIL6STOP
vIL6REV
B
PBS
vIL6STOP
vIL6REV
Ki67+ 8.88
Ki67+ 6.36
Ki67+ 16.4
Ki67
CD11c
CD16+ 5.50
CD16+ 4.19
CD16+ 12.3
CD16
29.4
62.0
80.7
PD-L1
C
Ki67+ %
CD16+ %
PD-L1+ %
0.0476
0.0302
0.0089
0.0009
D
PBS
LPS
vIL6REV
vIL6STOP
E
No infection
vIL6REV
vIL6STOP
vIL6
pSTAT1
pSTAT1 7.83
pSTAT1 49.9
pSTAT1 8.85
pSTAT1 9.53
pSTAT3
pSTAT3+ 5.74
pSTAT3+ 49.2
pSTAT3+ 4.79
pSTAT3+ 25.0

Figure 4

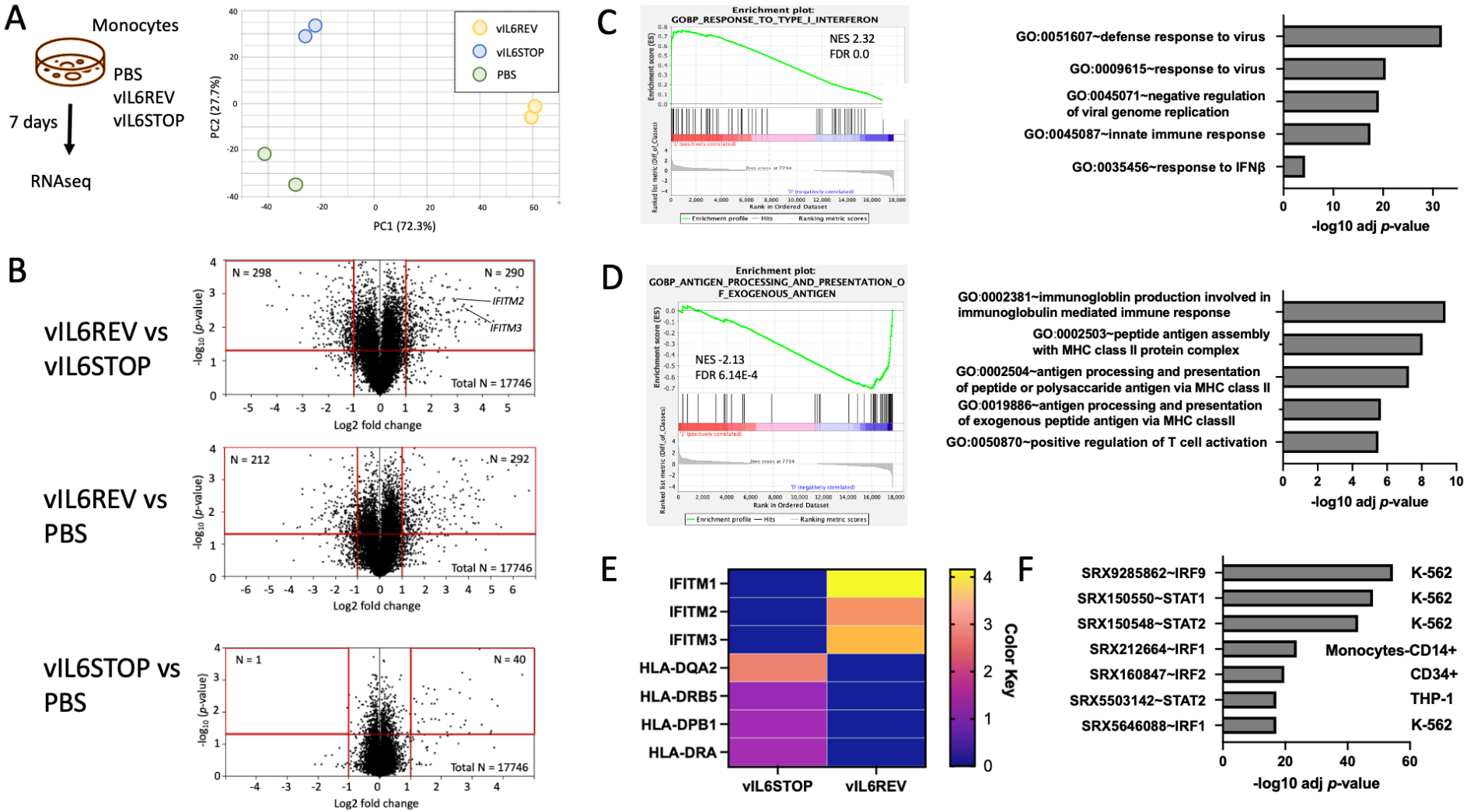
A
Monocytes
PBS
vIL6REV
vIL6STOP
7 days
RNAseq
vIL6REV
vIL6STOP
PBS
PC2 (27.7%)
PC1 (72.3%)
B
vIL6REV vs vIL6STOP
N = 298
N = 290
IFITM2
IFITM3
Total N = 17746
Log2 fold change
vIL6REV vs PBS
N = 212
N = 292
Total N = 17746
Log2 fold change
vIL6STOP vs PBS
N = 1
N = 40
Total N = 17746
Log2 fold change
C
Enrichment plot:
GOBP_RESPONSE_TO_TYPE_I_INTERFERON
NES 2.32
FDR 0.0
GO:0051607~defense response to virus
GO:0009615~response to virus
GO:0045071~negative regulation of viral genome replication
GO:0045087~innate immune response
GO:0035456~response to IFNβ
-log10 adj p-value
D
Enrichment plot:
GOBP_ANTIGEN_PROCESSING_AND_PRESENTATION_OF_EXOGENOUS_ANTIGEN
NES -2.13
FDR 6.14E-4
GO:0002381~immunogloblin production involved in immunoglobulin mediated immune response
GO:0002503~peptide antigen assembly with MHC class II protein complex
GO:0002504~antigen processing and presentation of peptide or polysaccaride antigen via MHC class II
GO:0019886~antigen processing and presentation of exogenous peptide antigen via MHC classII
GO:0050870~positive regulation of T cell activation
-log10 adj p-value
E
IFITM1
IFITM2
IFITM3
HLA-DQA2
HLA-DRB5
HLA-DPB1
HLA-DRA
vIL6STOP
vIL6REV
Color Key
F
SRX9285862~IRF9
SRX150550~STAT1
SRX150548~STAT2
SRX212664~IRF1
SRX160847~IRF2
SRX5503142~STAT2
SRX5646088~IRF1
K-562
K-562
K-562
Monocytes-CD14+
CD34+
THP-1
K-562
-log10 adj p-value

Figure 5

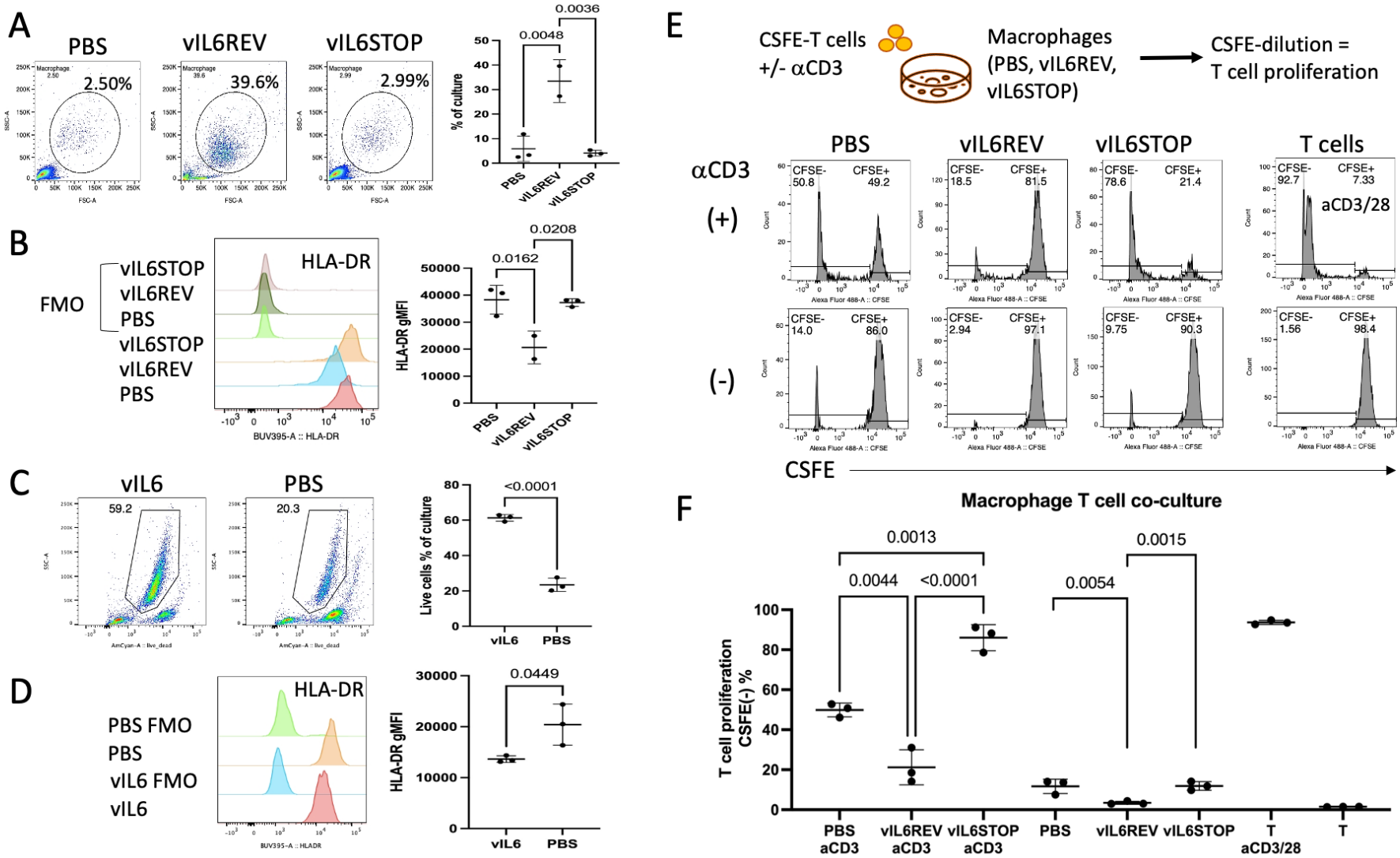
A
PBS
vIL6REV
vIL6STOP
2.50%
39.6%
2.99%
% of culture
0.0048
0.0036
B
FMO
vIL6STOP
vIL6REV
PBS
vIL6STOP
vIL6REV
PBS
HLA-DR
HLA-DR gMFI
0.0162
0.0208
C
vIL6
PBS
59.2
20.3
Live cells % of culture
<0.0001
D
PBS FMO
PBS
vIL6 FMO
vIL6
HLA-DR
HLA-DR gMFI
0.0449
E
CSFE-T cells
+/- αCD3
Macrophages
(PBS, vIL6REV,
vIL6STOP)
CSFE-dilution =
T cell proliferation
αCD3
(+)
(-)
PBS
vIL6REV
vIL6STOP
T cells
CFSE- 50.8
CFSE+ 49.2
CFSE- 18.5
CFSE+ 81.5
CFSE- 78.6
CFSE+ 21.4
CFSE- 92.7
CFSE+ 7.33
aCD3/28
CFSE- 14.0
CFSE+ 86.0
CFSE- 2.94
CFSE+ 97.1
CFSE- 9.75
CFSE+ 90.3
CFSE- 1.56
CFSE+ 98.4
CSFE
F
Macrophage T cell co-culture
T cell proliferation
CSFE(-) %
0.0013
0.0044
<0.0001
0.0054
0.0015
PBS aCD3
vIL6REV aCD3
vIL6STOP aCD3
PBS
vIL6REV
vIL6STOP
T aCD3/28
T